# FullBreathe: Full Human Respiration Detection Exploiting Complementarity of CSI Phase and Amplitude of WiFi Signals

YOUWEI ZENG, Peking University, China
DAN WU, Peking University, China
RUIYANG GAO, Peking University, China
TAO GU, RMIT University, Australia
DAQING ZHANG*, Peking University, China

Human respiration detection based on WiFi signals does not require users to carry any device, hence has drawn a lot of attention due to better user acceptance and great potential for real-world deployment. However, recent studies show that respiration sensing performance varies in different locations due to the nature of WiFi radio wave propagation in indoor environments, i.e., respiration detection may experience poor performance at certain locations which we call "blind spots".

In this paper, we aim to address the blind spot problem by investigating the property of both amplitude and phase information of WiFi signals as well as their relationship. Through a series of experimental studies, we discover an interesting phenomenon–amplitude and phase of WiFi channel state information (CSI) are perfectly complementary to each other. We reveal the mathematical model behind and exploit the complementary nature to design and implement a real-time respiration detection system with commodity WiFi devices. We conduct extensive experiments to validate our model and design. The results show that, with only one transceiver pair and without leveraging multiple sub-carriers, the system enable full location coverage with no blind spot, showing great potential for real deployment.

CCS Concepts: • **Human-centered computing → Ubiquitous and mobile computing systems and tools**;

Additional Key Words and Phrases: Respiration Sensing, WiFi, Channel state information (CSI)

**ACM Reference Format:**
Youwei Zeng, Dan Wu, Ruiyang Gao, Tao Gu, and Daqing Zhang. 2018. FullBreathe: Full Human Respiration Detection Exploiting Complementarity of CSI Phase and Amplitude of WiFi Signals. *Proc. ACM Interact. Mob. Wearable Ubiquitous Technol.* 0, 0, Article 39 (January 2018), 19 pages. https://doi.org/10.1145/nnnnnnn.nnnnnnn

*This is the corresponding author

Authors' addresses: Youwei Zeng, Key Laboratory of High Confidence Software Technologies (Ministry of Education), School of Electronics Engineering and Computer Science, Peking University, Beijing, China, ywzeng@pku.edu.cn; Dan Wu, Key Laboratory of High Confidence Software Technologies (Ministry of Education), School of Electronics Engineering and Computer Science, Peking University, Beijing, China, dan@pku.edu.cn; Ruiyang Gao, Key Laboratory of High Confidence Software Technologies (Ministry of Education), School of Electronics Engineering and Computer Science, Peking University, Beijing, China, gry@pku.edu.cn; Tao Gu, Computer Science and School of Science, RMIT University, Melbourne, Australia, tao.gu@rmit.edu.au; Daqing Zhang, Key Laboratory of High Confidence Software Technologies (Ministry of Education), School of Electronics Engineering and Computer Science, Peking University, Beijing, China, dqzhang@sei.pku.edu.cn.


2474-9567/2018/1-ART39 $15.00
https://doi.org/10.1145/nnnnnnn.nnnnnnn

## 1 INTRODUCTION

Chronic respiratory diseases (CRDs) are chronic diseases of the airways and other structures of the lungs. They affect 1 billion people in the world population, and account for 7% of all deaths worldwide (4.2 million deaths) [7]. Daily monitoring of respiration in a continuous and cost-effective way plays an important role in early diagnosis and treatment of CRDs, especially for people living alone at home. Traditional respiration detection technology requires patients to carry devices such as pulse oximeter [31] and capnometer [27] in a hospital setting. However, these devices are intrusive and may be bulky in size, hence they are impractical for long-term and continuous monitoring in a home setting. Several sensor-based systems have been proposed to minimize user discomfort, for example, systems leveraging on pressure sensor [38] or wearable sensor [28]. Although these systems are potentially deployable, the former can only detect respiration while subject lies on bed, and the latter may have the issues such as user acceptance or poor usability [12].

Compared to the systems replying on sensors, the device-free approach does not require user to wear any device, hence it may look more friendly and attractive to end users. This approach typically leverages on camera, acoustic and RF devices to sense respiration in a contactless manner. To name a few, a camera-based monitoring system is proposed in [6] to extract raw breathing signals from video stream. However, it requires direct line of sight (LoS) and good lighting condition. Smartphone's microphone is used in [29] to capture the acoustic information generated by breathing airflow for respiration detection. But this system has several critical drawbacks such as short sensing distance and being sensitive to environmental noise. RF-based technology has also been proposed to detect respiration such as Doppler radar [10], FMCW radar [3] and UWB radar [32]. These systems essentially exploit radio signals to measure tiny chest displacement during respiration. Although they have been shown to be both effective and accurate, they usually involve high deployment cost due to dedicated hardware, preventing them from practical use at home.

We have seen a recent trend of respiration monitoring based on widely available WiFi infrastructure in home settings. While WiFi received signal strength (RSS) signals are typically used in some systems [2], channel state information (CSI) signal has shown better performance due to its fine signal granularity, e.g., CSI amplitude used in [22–24, 39] and CSI phase difference between two antennas used in [36, 37]. Although these systems show great potential for real deployment, their performance is inconsistent because they are mostly experiment-based (i.e., an observation of rhythmical patterns caused by respiration) and lack of any theoretical justification. A recent study in [33] investigates the theory of Fresnel zone (FZ) to reveal radio wave propagation in WiFi. This theoretical model perfectly explains the performance fluctuation in existing systems, and reveals that human respiration cannot be sensed effectively when one stays in blind-spot locations. This study raises a key challenge–how to address the blind spot problem and ensure that respiration can be detected anywhere in the area covered by a transceiver pair. Although integrating multiple sub-carriers in CSI can alleviate this problem, there is no study showing that respiration sensing can be guaranteed both theoretically and experimentally due to the complex multi-paths in indoor environments. The most recent study in [34] uses multiple TX-RX antenna pairs to improve detectability leveraging on space diversity of antennas. Although sensing zones could be largely overlapped due to more antenna pairs deployed, such overlapping is random, and there is no evidence showing such overlapping can ensure a full coverage of respiration sensing in practical deployment.

This paper presents a novel solution to address the blind spot problem and ensure full respiration detection. We first conduct experiments to investigate respiration sensing based on CSI phase, and then discover that both interleaved detectable and undetectable regions exist when using CSI phase, similar to CSI amplitude [33]. Through our experiments, we find that, when CSI amplitude or CSI phase is used individually for respiration sensing, blind spots still exist in the coverage area. Interestingly, we reveal a phenomenon that the interleaved detectable regions of phase and amplitude are perfectly complementary to each other. In this paper, we prove mathematically that CSI amplitude and CSI phase follow perfect complementarity for full respiration detection.

To validate this theorem, we conduct extensive experiments in different indoor environments, different locations, and with different subjects. Based on this theorem, we design a system with commodity WiFi devices to enable full respiration detection with only one transceiver pair without leveraging multiple sub-carriers.

The main contributions of the work can be summarized as follows:

(1) We investigate the detectability of human respiration using WiFi CSI phase, and discover the phenomenon that its detectable and undetectable areas are interleaved in the physical space.
(2) We reveal and prove the perfect complementarity between CSI amplitude and phase, and validate this theorem through our experiments in different environments and locations with different subjects.
(3) We design and implement a full respiration detection system with commodity WiFi devices. To the best of our knowledge, this is the first work to achieve this goal using commodity WiFi devices.

The remaining of the paper is organized as follows. We first survey the state-of-art relevant to our work in Sec. 2, and provide the preliminary knowledge in Sec. 3. In Sec. 4, we first study respiration sensing with WiFi signals in the context of Fresnel zones, then explain the phenomenon that CSI amplitude and phase information are complementary to each other. Additionally, we show how to extend the complementarity property to phase-unsynchronized commodity WiFi devices for full-coverage respiration detection. We implement the prototype system in Sec. 5, and present our experimental design and evaluation results in Sec. 6 and discuss the limitation and opportunities in Sec. 7. Finally, we conclude our work in Sec. 8.

## 2 RELATED WORK

This section discusses the most relevant work in respiration sensing with RF signals which can be roughly divided into the following two categories.

**Radar-based respiration detection.** These approaches can be mainly divided into two categories according to the principles they use.

(1) Measuring the distance between chest and device directly. Since the chest displacement during respiration is minute (4.2-5.4 mm) [25], measuring such millimeter-level displacement using time of arrival related technologies requires ultra wide bandwidth. This category is always associated with sophisticated hardware such as FMCW radar[3, 4]. However, WiFi operates with a much lower bandwidth. For example, for a 802.11n Wi-Fi channel with 40 MHz bandwidth configuration, the signal is sampled once every 25 nanoseconds, during which the signal travels 7.5 meters. This ranging resolution is too coarse to track minute chest displacement, thus it is impossible to sense respiration in this way.
(2) Measuring the relative speed change or displacement. The UWB radar [8, 13, 14, 16] and CW Doppler radar [9, 11, 17, 18, 21, 26] have been used to analyze the Doppler effect induced by subject's movement, and have been widely deployed in applications such as vehicle speed estimation. When applying the Doppler effect to detect minute-level movement such as human respiration, it arises several additional challenges. One of them is that the blind spots (a.k.a. null detection points) where the respiration cannot be detected reliably. Several solutions have been proposed leveraging quadrature demodulation [11], and frequency tuning technique in double-sideband system[42]. However, as the transceivers of commodity WiFi are not tightly time-synchronized, they are quite different from the radar counterparts. As a result, neither of these two techniques can be applied to respiration sensing with WiFi. The reason is two-folds. Different from CW Doppler radar, CSI measurement suffers from serious phase distortion, resulting in frequency offset in I/Q outputs from quadrature demodulation. Besides, we are not able to tune frequency in WiFi as freely as we do in CW Doppler radar.

**WiFi-based respiration detection.** These WiFi-based approaches can be divided into two categories as follows.

(1) Pattern-based respiration detection. Inspired by an observation that the RSS at a WiFi-enabled device held on a person's chest is affected by the breathing process, Abdelnasser *et al.* [2] leverage these changes in the WiFi RSS patterns to extract respiration rate. However, RSS is insensitive to the minute chest movements during respiration and can be easily overwhelmed by noise [24]. These drawbacks prevent it from detecting respiration reliably in natural settings.
Compared to RSS, CSI is more sensitive to human respiration. Wi-Sleep [23] appears to be the first work to exploit WiFi CSI information for respiration detection during sleep. This work is then extended in [24] where the sleeping postures and abnormal breathing patterns are considered. Liu *et al.* [22] further propose to track both respiration rate and heart rate during sleep. Wu *et al.* [39] extend respiration detection from sleeping to standing posture for stationary human detection. While they utilize WiFi CSI amplitude for respiration detection, TensorBeat [37] and PhaseBeat [36] exploit WiFi CSI phase difference between two receiver antennas to extract respiration rate and heart rate. PhaseBeat has shown to achieve a considerably higher accuracy than the amplitude based method for breath rate estimation. These systems are mainly based on the periodicity of signal patterns, but they are unaware of why human respiration would lead to very different, even irregular waveforms. There is no study investigating how human respiration can be detected reliably anywhere in the area.
(2) Model-based respiration detection. These approaches relate one's chest movement to the received WiFi signals and models respiration sensing as a mathematical problem. A recent paper [33] introduces the Fresnel zone model to explain why and when respiration can be sensed with WiFi signals. The Fresnel zone model shows there exists some blind spots. Wang *et al.* [34] use multiple transceiver pairs to enhance the ability to capture human respiration, and use overlapped Fresnel zones to overcome this problem. However, they both essentially leverage on amplitude information, and blind spots still exist.

In this work, we aim to address the blind spot problem and ensure full respiration detection with commodity WiFi devices.

## 3 PRELIMINARY

In this section, we present some background information for this work.

### 3.1 Radio Signal Propagation

Radio wave signal in an indoor environment propagates from the direct path and massive multi-paths caused by reflection, diffraction and scattering. The received signal strength is the superposition of all the path components. For a radio wave with a wavelength of $\lambda$, when it travels along a path with length of $d$, its phase shifts by $2\pi d/\lambda$. The total received signal can thus be expressed as $\sum a_i e^{-j2\pi d_i/\lambda}$, where $i$ is the path identifier number and $a$ is the attenuation coefficient of each path.

### 3.2 Overview of CSI

The phase shift and power attenuation characterize the signal propagation properties for a single frequency in a specific environment. Specifically, CSI characterizes wireless channel by presenting Channel Frequency Response (CFR) of each sub-carrier. A CFR value of CSI contains complex information, in which its amplitude represents magnitude and phase represents angle information. Channel state $H(f,t)$ for carrier frequency $f$ has the relation of $Y(f,t) = H(f,t)X(f,t)$, where $X(f,t)$ and $Y(f,t)$ are the transmitted signals and received signals, respectively, in the frequency domain.

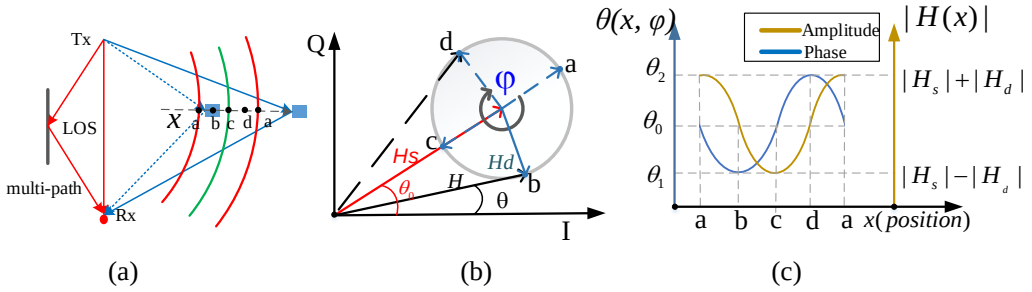


Fig. 1. Illustrations of CSI phase and amplitude change patterns when a subject moves towards outer FZs (from location *a* to location *b, c, d*): (a) an object moves across the boundaries of FZ in a multi-path environment, where the thick red (green) line represents the odd (even) boundary of FZ. (b) the phasor representation of CSI is composed of a static component $H_s$ and a dynamic component $H_d$. As an object moves outward, the phase of $H_d$ increases and rotates from point *a* to *b,c,d*. (c) CSI phase and amplitude waveforms with respect to different object locations.

### 3.3 Fresnel Zone

The Fresnel zone (FZ) model was originated from the optics research. Wu *et al.* [41] and Wang *et al.* [33] first introduced the Fresnel zone (FZ) model for WiFi based wireless sensing, and studied the relationship between human motion and the received signals. In their study, several interesting findings are presented. When an object moves across a series of the FZs, the received signal shows a continuous sinusoidal-like waveform. If the reflected path length change caused by a moving object is shorter than one wavelength, the received signal is just a fragment of the sinusoidal-like waveform. Human respiration typically results in a minute chest movement, thus may only cause reflected path length to change less than one wavelength. Apparently, to detect respiration effectively, it is required that the signal lies fully in the monotonically changing fragment. Based on the above study, Wang *et al.* [33, 40, 44] conclude that, for respiration sensing with CSI amplitude, the best location appears in the middle of FZ, while the worst location is at the boundary of FZ.

## 4 RESPIRATION SENSING WITH PHASE AND AMPLITUDE INFORMATION

In this section, we propose to combine CSI phase and amplitude information for full respiration detection. First, we explore to sense respiration with CSI phase. Next, we show CSI phase and amplitude are complementary to each other theoretically. Finally, We verify the complementarity property through experiments, and show how to extend this property to commodity WiFi devices with CSI phase distortions.

### 4.1 Respiration Sensing by CSI phase

As illustrated in Fig. 1 (a), in a device-free passive respiration sensing scenario, a WiFi transceiver pair is placed at a fixed location and an object moves towards outer FZs. As introduced in Sec. 3.1 and Sec. 3.2, CSI is the superposition of components from all the paths a radio wave travels through, which can be divided into static and dynamic components according to prior work [33, 35, 41]. In this scenario, the static component is composed of the LoS propagation and other reflection paths from static objects in the environment while the dynamic component is the path reflected from the chest of a subject. Apparently, the static component is affected by the surrounding environment and the LoS of transceivers while the dynamic component is determined by the reflection path from chest. Mathematically, the total CSI can be denoted as follows [33, 35, 41]:

$$H(f,t) = H_s(f,t) + H_d(f,t) = H_s(f,t) + A(f,t)e^{-j2\pi\frac{d(t)}{\lambda}} \quad (1)$$

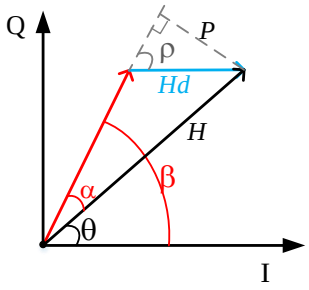


Fig. 2. Derivation of the formula of CSI phase

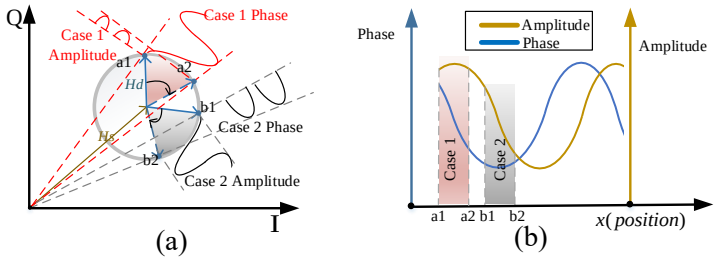


Fig. 3. Conceptual illustration of the complementarity between CSI amplitude and phase at two positions–boundary (light red) and middle (light gray) of FZs: (a) CSI phasor diagram shows the sensitivity of phase and amplitude are different for the two positions. (b) phase and amplitude waveform fragments w.r.t the two positions.

where $H_s(f,t)$ is the static component, $A(f,t)$, $e^{-j2\pi\frac{d(t)}{\lambda}}$ and $d(t)$ are the attenuation, the phase shift and the path length of dynamic component $H_d(f,t)$, respectively.

We now analyze CSI phase change patterns while the reflection path length increases gradually. As shown in Fig. 1 (b), based on the trigonometric geometry, CSI phase gets its minimum value $\theta_1$ and maximum value $\theta_2$ at two tangent positions (point $b$ and $d$ in Fig. 1, respectively) in the circle formed by the rotation of dynamic component, corresponding to the middle of FZ. While a subject moves continuously, the phase of CSI changes between $\theta_1$ to $\theta_2$ accordingly. Based on Equ. 1 and Fig. 2, the time-varying CSI phase can be notated as:

$$\theta = \beta - \alpha = \beta - \arcsin\frac{P}{|H|} = \angle H_s - \arcsin\frac{|H_d|\sin\rho}{\sqrt{|H_s|^2 + |H_d|^2 + 2|H_s||H_d|\cos\rho}} \tag{2}$$

where $\beta$ is the phase of static component $H_s$, $\alpha$ is the phase difference between the total CSI $H$ and $H_s$, $P$ is the distance from the edge of dynamic component $H_d$ to $H_s$, $|H|$ is the total CSI amplitude and $\rho$ is the Fresnel phase, which is basically the phase difference between the dynamic component and the static component [41]. Since $|H_d|\sin\rho$ is a small value compared to $|H_s|$ [20], we approximate CSI phase as follows:

$$\theta \approx \angle H_s - \frac{|H_d|}{\sqrt{|H_s|^2 + |H_d|^2 + 2|H_s||H_d|\cos\rho}}\sin\rho \tag{3}$$

Note that $|H_d|$ is quite smaller than $|H_s|$, the item $\cos\rho$ in the denominator has almost no effect on the second item to the right of Equ. 3. Thus the CSI phase is mainly determined by $\sin\rho$, and the waveform of CSI phase is a sinusoidal-like waveform.

Based on the definition of CSI phase and amplitude, we conduct simulations and plot the CSI phase and amplitude waveforms according to the boundaries of FZ in Fig. 1 (c). We observe that, CSI phase changes very little in the middle of FZ (point $b$ and $d$ in Fig. 1), but more significantly at the boundary of FZ (point $a$ and $c$ in Fig. 1). This suggests that, while using CSI phase for respiration sensing, the best subject location should be right at the boundary of FZ and the worst location should be in the middle of FZ. Thus, during the period in which the reflection path length changes one wavelength, the phase of dynamic component rotates by $2\pi$, and two undetectable regions (around the middle of FZ) and two detectable regions are expected. In addition, the detectable and undetectable regions are interleaved.

### 4.2 Complementarity between CSI Phase and Amplitude

Based on our analysis above, respiration cannot be detectable in all the locations when amplitude or phase is used individually. In this section, we first present an interesting phenomenon that the interleaved detectable regions for phase and amplitude are perfectly complementary to each other, and then reveal the theory behind.

We make the same assumption as in [33] that a normal respiration causes the phase of dynamic component to change about $\pi/3$ (60 degrees). We first study two cases to observe how CSI amplitude and phase vary during respiration over time, as shown in Fig. 3 (a).

(1) In Case 1, a subject is located at the boundary of FZ. During exhaling, the dynamic component rotates from $a_1$ to $a_2$. The minute and non-monotonic change in amplitude makes it hard for respiration detection, but it can be detected by using CSI phase.
(2) In Case 2, a subject is located in the middle of FZ. During exhaling, the dynamic component rotates from $b_1$ to $b_2$. Respiration can be detected by amplitude, but not phase.

We observe that a bad location for amplitude sensing turns out to be a good position for phase sensing, and vice versa. To further understand this phenomenon, we take a close look at a complete waveform of CSI amplitude and phase which contains one period, as shown in Fig. 3 (b). We wonder if there is a situation when both amplitude and phase change non-monotonically. Actually, this case does not exist and the reason could be explained as follows. Based on the definition of CSI phase and amplitude, we can easily find that CSI amplitude is a cosinusoidal-like function of the Fresnel phase while CSI phase is a sinusoidal-like function of the Fresnel phase, as shown in Fig. 1 (c). The sinusoidal-like and cosinusoidal-like waveforms have a phase difference of $\pi/2$. For a fragment less than 1/4 period, it is impossible to get non-monotonic regions for both phase and amplitude. Thus a situation when both CSI amplitude and phase are undetectable for respiration does not exist.

Now, we dive deeper to reveal the inside of the complementarity nature of CSI amplitude and phase. During human respiration, the dynamic component rotates and CSI changes along a circular arc. Since phase and amplitude are two orthogonal bases of the complex CSI value, the change of CSI could be represented by these two bases. If there is little change observed from one basis, then it must be obvious observed from another basis. We conclude that the situation when both basis have little change does not exist. This situation occurs only if CSI does not change. It contradicts with the assumption that any moving object causes changes of the dynamic component. So it is guaranteed that at least one of CSI phase and amplitude can be used to detect respiration regardless of subject's position, provided the subject is within the WiFi sensing range.

The analysis above has shown that, as long as the surrounding environment and the placement of transceivers are determined, the complementarity of phase and amplitude is irrelevant to subject's position. Actually, the complementary property is intrinsic for respiration sensing, it holds in different environment with different placement of transceiver, and is resilient to the environmental changes. To understand the reason why the complementarity property does not change with the environment, we study how the parameters in real world affect our model. A subject's location affects both the magnitude and phase of dynamic component. As long as the subject is within the sensing range, the magnitude of dynamic component is larger than zero. We have discussed before that at any location inside FZ, respiration is always detectable. The displacement of antennas and the room layout affect the distribution of multi-paths, which further changes the static component. So do any environmental changes, for example, an object move from one place to another. The change of static component affects the initial Fresnel phase. Both the changes of static component and dynamic component only affect the selection between phase and amplitude for respiration sensing, but not the complementarity.

### 4.3 Verifying Respiration Sensing with CSI Phase and Amplitude

In this section, we intend to verify the proposed model for respiration sensing with CSI phase and amplitude through experiments.

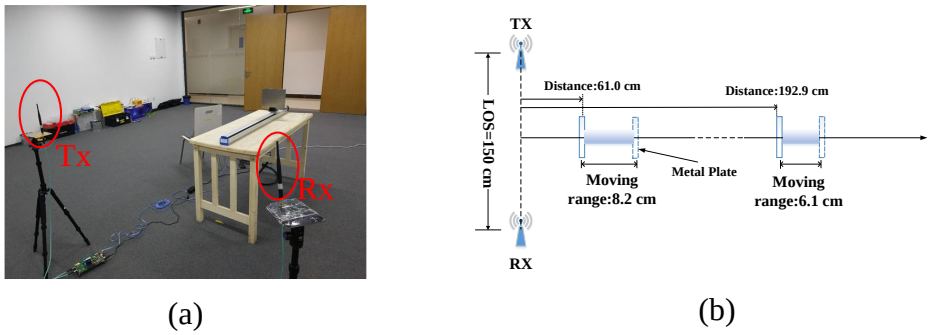


Fig. 4. Experimental settings to verify the proposed model in two different regions, i.e., a distance relatively near to the LoS (from 61.0 cm to 69.2 cm) and a far counterpart (from 192.9 cm to 199.0 cm).

**Experimental settings:** In these experiments, we use the Rice WARP platform [1] and configure the WiFi transceiver at a frequency of 5.31 GHz. We use the same synchronized clock for all the WARP RF chains to remove phase distortion between transceivers so that accurate phase can be obtained.

We separate the transceivers 150 cm apart to conduct experiments. In order to control the object's position precisely, we use a metal plate mounted on a high precision THK programmable linear motion slider to simulate the chest displacement during respiration. The slider can set the start and stop endpoints with a localization precision of 0.01 mm, and the moving speed of the metal plate can be carefully controlled to simulate respiration, as is shown in Fig. 4 (a). The slider is arranged perpendicular to the LoS between transceivers. In our setting, the displacement for each move of the metal plate is set to 5 mm, which is on a par with the chest displacement during respiration.

As shown in Fig. 4 (b), we conduct two sets of experiments at two locations, i.e., one distance relatively near to the LoS and the other relatively far. The reason to choose two different places is that we want to observe how the unevenly distributed spatial interval of FZs affect respiration detectability. From a geometrical perspective, the spatial interval between two adjacent FZs near to the LoS is larger than that of the far ones. In each case, the metal plate moves 5 mm back and forth periodically, and we record the CSI data. After that, the metal plate moves 0.5 mm outward to arrive at the next position in sequence. We repeat this process until the reflection path length changes about two wavelengths. Specifically, the metal plate moves gradually from 61.0 cm to 69.2 cm in the near region case, while it moves from 192.9 cm to 199.0 cm in the far region case. In each case, the change covers two periods and the total CSI rotates by $4\pi$. It is guaranteed that all possible combinations of CSI phase and amplitude are included in the experiments. We conduct the experiments to verify: 1) the detectable and undetectable regions of CSI phase appear alternately, and the undetectable regions appear exactly twice during the period in which the reflection path length changes one wavelength; 2) the undetectable regions of CSI phase and amplitude are complementary to each other for full respiration detection. A waveform is considered detectable for respiration if it is a (co)sinusoidal-like waveform with clear periodic patterns and its periodicity is in line with the ground-truth (about 2.5 cycles in this setting).

**Experimental results:** (1) Fig. 5 (a) shows 8 selected CSI phase waveforms inside the near region from 61.0 cm to 69.2 cm. We can observe that the detectable and undetectable areas of CSI phase appear alternately. Since the reflected path length changes two wavelengths, there are 4 detectable regions (positions 1, 3, 5, 7 in Fig. 5 (a)) along with 4 undetectable regions (positions 2, 4, 6, 8 in Fig. 5 (a)). In the far region case, the metal plate moves from 192.9 cm to 199.0 cm. The results are similar, as shown in Fig. 5 (b). The difference is that, the distance between its detectable and undetectable regions is approximately 0.75 cm, which is smaller than 1 cm in the near

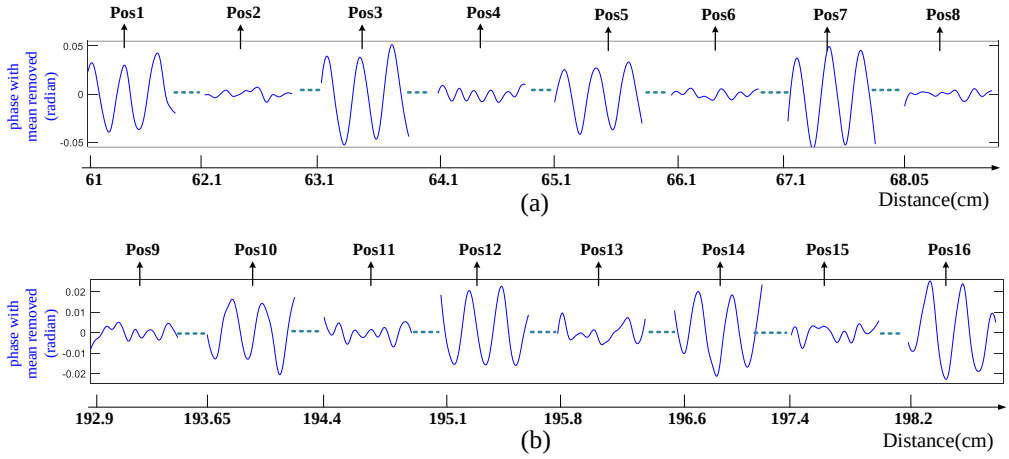


Fig. 5. CSI phase change patterns at 8 consecutive positions during the period in which the reflected path length changes two wavelengths, the distance on x axis indicates the start position of each movement of 5 mm: (a) a distance relatively near to the LoS. (b) a distance relatively far from the LoS.

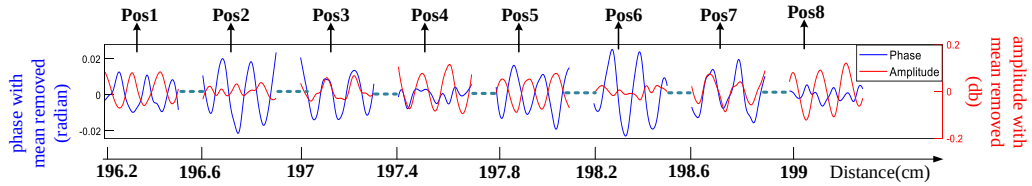


Fig. 6. CSI phase and amplitude change patterns at 8 consecutive positions during the period in which the reflected path length changes one wavelength.

region. This is expected, since the FZ is unevenly distributed spatially, i.e., the interval between two adjacent inner FZs is larger than the outer FZs.

(2) Fig. 6 presents 8 selected CSI waveforms of phase and amplitude combined for the metal plate moves from position 196.2 cm to 199.0 cm, during which the reflected path length changes one wavelength. In this setting, all the possible combinations of detectability of CSI phase and amplitude shown in Sec. 4.2 are included in Fig. 6: i) both phase and amplitude are detectable (positions 1, 3, 5, 7 in Fig. 6); ii) phase is detectable while amplitude is undetectable (positions 2, 6 in Fig. 6); iii) amplitude is detectable while phase is undetectable (positions 4, 8 in Fig. 6). And the experiment in the near region gets the similar result. Please be aware that although both amplitude and phase can detect respiration at positions 1, 3, 5, 7, CSI amplitude and phase appear to fluctuate in-phase at positions 3, 7, while out-phase at positions 1, 5. As illustrated in Sec. 4.1, positions 2, 4, 6, 8 in the experiment are corresponding to positions a, b, c, d in Fig. 1, while the positions 3, 5, 7, 1 in the experiment are corresponding to the intervals in between positions a, b, c, d, a in Fig. 1.

### 4.4 Extend the Complementarity to the Commodity WiFi

The complementarity of CSI phase and amplitude presented in Sec. 4.2 can be used to build a full respiration detection system, as long as we can obtain accurate CSI. Unfortunately, the CSI measurement in commodity WiFi

suffers from several phase offsets [15, 19, 43, 46], which makes CSI phase totally random across consecutive CSI samples, thus breaks the complementarity property. In this section, we show how MIMO technology is utilized to extend the complementarity property to commodity WiFi.

*4.4.1 Removing the Random Phase Offset.* For commodity WiFi, the clock-unsynchronized transceivers result in a time-varying random phase offset $e^{-j\theta_{offset}}$ in each CSI sample as shown as follows:

$$H(f,t) = e^{-j\theta_{offset}}(H_s(f,t) + A(f,t)e^{-j2\pi\frac{d(t)}{\lambda}}) = e^{-j\theta_{offset}}(S(f,t)e^{-j\alpha(t)} + A(f,t)e^{-j2\pi\frac{d(t)}{\lambda}}) \tag{4}$$

where $H_s(f,t)$ is the static component, $S(f,t)$ is the attenuation, $\alpha(t)$ is phase shift of static component, and $A(f,t)e^{-j2\pi\frac{d(t)}{\lambda}}$ is the dynamic component.

Several solutions have been proposed to recover CSI phase from commodity WiFi [43, 45]. The recovery process involves the fix to sampling frequency offset (SFO) and carrier frequency offset (CFO). However, both the phase recovery methods require the object moves larger than one wavelength, rendering it unsuitable for the sub-wavelength level respiration detection. Fortunately, the time-varying random phase offsets are the same across different antennas on a WiFi card [15, 19], since they share the same RF oscillator. Thus, we apply conjugate multiplication (CM) of CSI between two antennas to remove the time-varying random phase offsets [20]:

$$\begin{aligned} H_{cm}(f,t) &= H_1(f,t)\overline{H_2(f,t)} \\ &= (S_1e^{-j\alpha_1} + A_1(f,t)e^{-j2\pi\frac{d_1(t)}{\lambda}})(S_2e^{j\alpha_2} + A_2(f,t)e^{j2\pi\frac{d_2(t)}{\lambda}}) \\ &= \overbrace{S_1S_2e^{-j(\alpha_1-\alpha_2)}}^{①} + \overbrace{S_2e^{j\alpha_2}A_1(f,t)e^{-j2\pi\frac{d_1(t)}{\lambda}}}^{②} \\ &+ \overbrace{S_1e^{-j\alpha_1}A_2(f,t)e^{j2\pi\frac{d_2(t)}{\lambda}}}^{③} + \overbrace{A_1(f,t)A_2(f,t)e^{-j2\pi\frac{d_1(t)-d_2(t)}{\lambda}}}^{④} \end{aligned} \tag{5}$$

where $H_{cm}(f,t)$ is the output of conjugate multiplication (CM), $H_1(f,t)$ is CSI of the first antenna and $\overline{H_2(f,t)}$ is the conjugate of CSI of the second antenna.

*4.4.2 Complementarity of Phase and Amplitude of Conjugate Multiplication.* From Equ. 5, we know that, the conjugate multiplication (CM) $H_{cm}(f,t)$ consists of four components, namely ①, ②, ③ and ④. The product of static components ① can be treated as a constant, and the product of dynamic components ④ is a small value which can be ignored. The remaining terms ② and ③ are two products of static component of one antenna and dynamic component of another antenna, which contain the respiration information we care about.

Please note that, while a person breathes normally, only $d_1(t)$ and $d_2(t)$ changes in Equ. 5. Since the two close-by antennas have the similar reflection path, their reflection path length change can be seen as the same during respiration. That is to say, the difference of reflection path length between two antennas $d_1(t) - d_2(t) = \Delta d$ is constant. Then we can rewrite the superposition of item ② and ③ as:

$$\begin{aligned} ② + ③ &= S_2e^{j\alpha_2}A_1(f,t)e^{-j2\pi\frac{d_1(t)}{\lambda}} + S_1e^{-j\alpha_1}A_2(f,t)e^{j2\pi\frac{d_2(t)}{\lambda}} \\ &= S_2e^{j\alpha_2}A_1(f,t)e^{-j2\pi\frac{d_1(t)}{\lambda}} + S_1e^{-j\alpha_1}A_2(f,t)e^{j2\pi\frac{d_1(t)-\Delta d}{\lambda}} \\ &= M_-e^{-j\gamma_-}e^{-j2\pi\frac{d_1(t)}{\lambda}} + M_+e^{-j\gamma_+}e^{j2\pi\frac{d_1(t)}{\lambda}} \end{aligned} \tag{6}$$

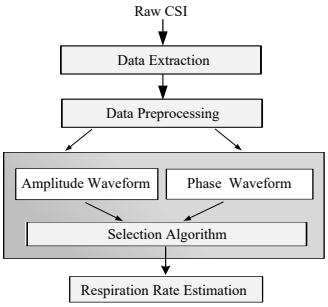


Fig. 7. System Overview

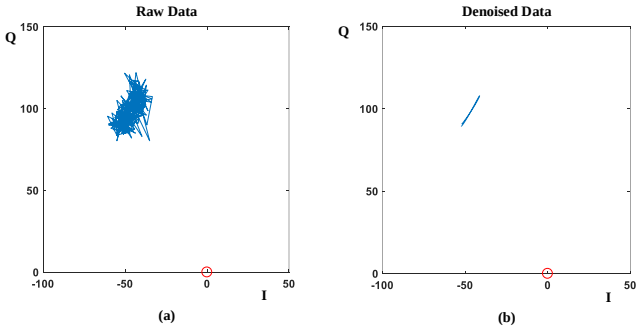


Fig. 8. The CM data in complex plane when a subject breathes normally: (a) raw data. (b) denoised data using Savitzky-Golay smoothing.

where $M_{-}e^{-j\gamma_{-}} = S_2 e^{j\alpha_2} A_1(f,t)$, $M_{+}e^{-j\gamma_{+}} = S_1 e^{-j\alpha_1} A_2(f,t) e^{-j2\pi \frac{\Delta d}{\lambda}}$ are both constant. According to [30], Equ. 6, which is the superposition of two components with opposite rotation directions, represents an ellipse in the complex plane. Therefore, when a subject breathes, the locus of CM is an arc on the ellipse.

As for respiration sensing, the difference between the CSI of a single antenna and the CM of CSI between two antennas lies in that, the former is an arc of circle in the complex plane while the latter is an arc of ellipse. Since the ellipse could be thought as a deformed circle in shape, it keeps most properties of the circle. Thus, the complementarity of CSI phase and amplitude still holds for ellipse as for circle, and the complementarity property can be easily extended to the CM.

## 5 SYSTEM DESIGN AND IMPLEMENTATION

In this section, we present our design and implementation of a real-time respiration monitoring system named FullBreathe. The system consists of four modules: Data Extraction, Data Preprocessing, Data Stream Selection and Respiration Rate Estimation, as shown in Fig. 7.

### 5.1 Data Extraction

CSI data is collected from two antennas of the same receiver. We have shown in Sec. 4.4.2 that the transceivers of commodity WiFi are not clock-synchronized. We thus choose CM of CSI between two Rx antennas as input.

### 5.2 Data Preprocessing

Data preprocessing involves data denoising and normalization. Raw CSI data collected at commodity WiFi is noisy, thus data denoising is required to obtain smooth and clear input data. Savitzky-Golay filter, which fits successive subset of data points with low degree polynomial by the method of linear least square, has shown its advantage in keeping the shape of waveforms and introduce less distortion than band-pass filters in the previous researches [5, 41]. We use Savitzky-Golay filter to smooth the data, as shown in Fig. 8. Please note that it is important to keep the shape of waveforms for respiration rate estimation using peak identification, which will be introduced in Sec. 5.4.

After denoising, we split the denoised data into two streams, one for its amplitude and the other for its phase. Note that amplitude and phase are in different fundamental units. For example, when a person breathes normally, the change in amplitude may be within 1 db while that in phase may be within 0.05 rad. Hence, we adopt standard score (a.k.a. z-score) to normalize the amplitude and phase so that they are comparable to each other, as shown in Fig. 9.

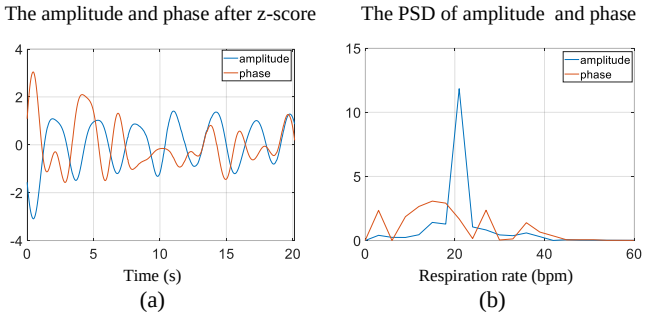


Fig. 9. The illustration of data stream selection among amplitude and phase: (a) the amplitude and phase of CM after z-score. (b) the PSD of amplitude and phase. In this case, the amplitude is selected for respiration rate extraction.

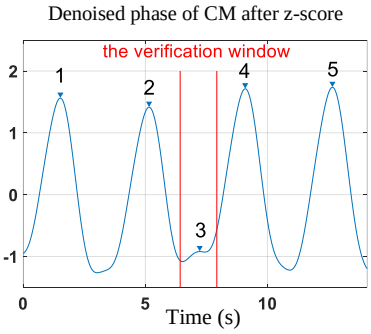


Fig. 10. Illustration of fake peak removal

## 5.3 Data Stream Selection

Based on our analysis in Sec. 4.3, at least one stream is capable of detecting respiration effectively. Therefore, we set criteria to determine which stream contains better respiration information we want. To decide which stream is better, we extract features from their power spectral density (PSD) using FFT, which transforms the time-domain data stream into its corresponding frequency-domain counterpart. Note that the amplitude and phase have the same total power in their PSD after standard score. Since a better one is a sinusoidal-like waveform, it is expected to observe a sharp peak in the range of normal respiration rate (10 bpm to 37 bpm) [22] from its PSD. In addition, for a better wave stream, most of the power is concentrated on the sharp peak, leading to a higher variance, as shown in Fig. 9 (b).

Based on the analysis above, we first check whether the amplitude or phase get their maximum value from 10 bpm to 37 bpm in their PSD. If only one satisfies this criteria, then it is what we want. If both of them satisfy this criteria, we compare their variance of PSD and choose the one that has the higher variance. Taking Fig. 9 for example, the amplitude of CM is selected according to our selection algorithm.

## 5.4 Respiration Rate Estimation

After selection of data streams, we apply the peak identification used in [22] to extract respiration rate. The FFT method is not used because its frequency resolution depends on the window size of FFT [3]. For example, for a window size of 20 seconds, the resolution of respiration rate estimation is 0.05 Hz, i.e., 3 breaths/minute. Although a larger window size helps to increase the resolution, it will also lead to a lower time domain resolution [36].

We estimate the respiration cycle by calculating the peak-to-peak time intervals of the selected waveform in a window size of 20 seconds. However, the peak identification method is sensitive to the unsmoothed waveform, and its performance will degrade dramatically if the fake peaks are involved in the peak-to-peak time intervals calculation. We apply the fake peak removal algorithm proposed in [22] to delete the fake peaks from all the peak candidates. A peak is considered as a fake peak if it is not the maximum value compared to all its neighbor samples within a verification window. In our implementation, the verification window size is 1.5 seconds centered at the peak. As shown in Fig. 10, there are 5 peak candidates totally, from peak 1 to peak 5. We can observe that, peak 3 is not the maximum value in the verification window, thus it is a fake peak and should be excluded. Therefore, there are only 4 actual peaks corresponding to respiration.

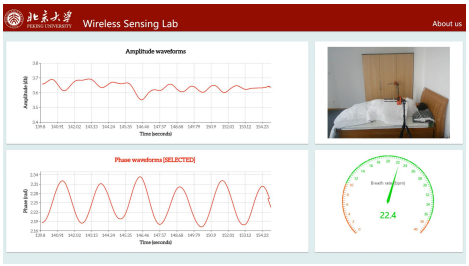


Fig. 11. Web-based user interface of FullBreathe system.

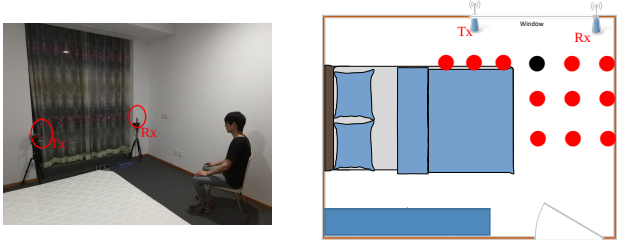


(a) (b)

Fig. 12. Experimental setting to verify the complementarity of phase and amplitude of CM at 12 different locations in: (a) a bedroom. (b) floor plan of the bedroom with 12 testing locations.

After the fake peak removal, we can extract respiration rate from those actual peaks. Assuming that the waveform gets its actual peaks at time $\tau_1, \tau_2, ..., \tau_n$, then the estimated respiration rate is:

$$60 \cdot \frac{1}{\frac{1}{n-1}\sum_{i=1}^{n-1}(\tau_{i+1} - \tau_i)} \tag{7}$$

where the factor of 60 transforms the frequency unit from Hz to breaths/minute.

## 6 EVALUATION

In this section, we demonstrate the complementarity of CSI phase and amplitude for respiration sensing with commodity WiFi devices in real-world deployment. We present our experimental settings in Sec. 6.1. After that, we evaluate the detectable and undetectable areas are alternatively distributed in space when using only the phase of CM, and the complementarity property still holds for the CM in Sec. 6.2. At last, in Sec. 6.3, we analyze the factors that may have influence on respiration detection, and evaluate the proposed model in realistic environments.

### 6.1 Experimental Settings

FullBreathe requires one WiFi transmitter and one receiver. We employ GIGABYTE mini-PCs equipped with off-the-shelf Intel 5300 wireless NIC card as transceivers. The transmitter is equipped with one omni-directional antenna while the receiver is equipped with two omni-directional antennas. The WiFi is configured to run at a frequency of 5.745 GHz. We collect CSI in a sampling rate of 100 Hz, and we use MATLAB for data processing. The ground-truth is recorded by a NeuLogg respiration monitor belt logger sensor NUL-236. We build an on-line web-based user interface to show breath rate along with a real-time video stream, shown in Fig. 11. We recruit 8 student volunteers to participate in all the experiments, including 5 males and 3 females, aging from 18 to 31.

### 6.2 Verifying the Complementarity with Commodity WiFi

In this section, we verify that the complementarity property could be extended to commodity WiFi with the method proposed in Sec. 4.4. In this experiment, the transmitter and receiver are placed with the LoS distance set to 1.9 m apart in a bedroom, as shown in Fig. 12 (a), and the subject is instructed to sit on the chair facing the transceivers and breathe normally.

We instruct the subject to sit at 12 different locations, as shown in Fig. 12 (b). Since it is difficult to control a subject's position as accurately as we did in the controlled experiment in Sec. 4.4, in each location, instead of moving a subject's location bit by bit each time, we mount the transmitter and receiver antennas on two sliders

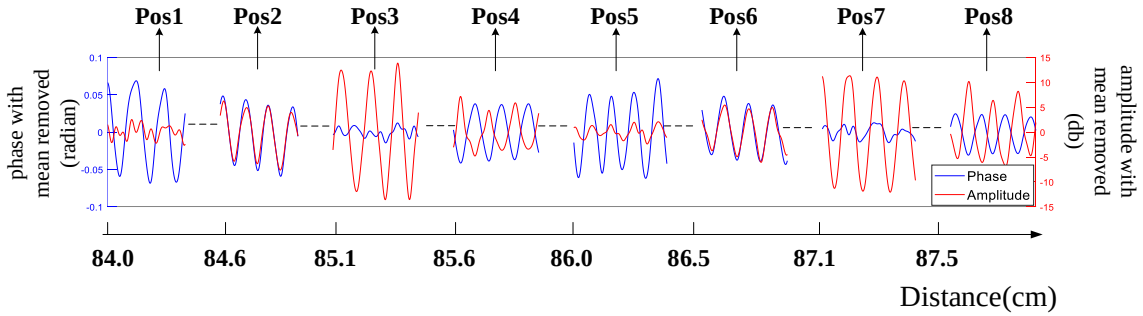


Fig. 13. Phase and amplitude change patterns of the CM data on commodity WiFi devices. we can see both phase and amplitude have undetectable regions when used individually, but at least one of them is guaranteed to detect respiration reliably.

attached to the tripods and move the antennas, in order to change the subject's position relative to the transceivers more accurately. Please note that, both antennas of transmitter and receiver are moved synchronously with the LoS between the transceivers keeping the same. For each location, we conduct a set of experiments to verify the phase and amplitude are complementary to each other for full respiration sensing. Similar to what we did in Sec. 4.4, we move the antennas outward for approximately 0.1 cm each time for CSI data collection and repeat the process, and we adjust the position of antennas gradually so that the reflected path length changes two wavelengths. In this process, the subject crosses 4 FZs and the CM of CSI rotates by $4\pi$, so that all the possible combinations of phase and amplitude are recorded in the experiments.

Fig. 13 presents eight selected data streams of phase and amplitude putting together for subject sitting at location 1 when the antennas move to eight different positions sequentially so the reflected path length changes one wavelength. As shown in Fig. 12 (b), location 1 labeled in black is relatively near to the LoS. We can observe that, for phase and amplitude of CM, the detectable and undetectable areas are alternatively interleaved, respectively, and when the reflected path length changes one wavelength, the undetectable regions appear twice. We can see that, for each streams, the undetectable region of phase and amplitude is complementary to each other. The experimental result in all the other eleven locations show similar results as in location 1, which we will not show the results here. Through these experiments we know it is very similar to that in Sec. 4, and the complementarity property of the CM still holds regardless of subject's positions.

## 6.3 Impact of Various Factors

In this section, we analyze all the factors that may have influence on respiration detection, and evaluate the proposed model in realistic environments.

As shown in Sec. 4.1, CSI is the superposition of components from all the paths which a radio wave travels through, and can be divided into the static and dynamic components. The static component is composed of the LoS path and the paths reflected from the static objects in the environment, while the dynamic component is the path reflected from the chest of a subject. By fixing the location of antennas and the surrounding environment, we have verified the influence of dynamic component in the previous section and comfirmed the property of complementarity. Next, we study the impact from static component: 1) the LoS distance of the transceivers. 2) different rooms. 3) the environmental changes.

For brevity, we present the experimental results by the detectability ratio metric rather than the detailed waveforms. The detectability ratio is defined as $\frac{N_{detectable}}{N_{all}}$, where $N_{detectable}$ is the number of CSI measurements

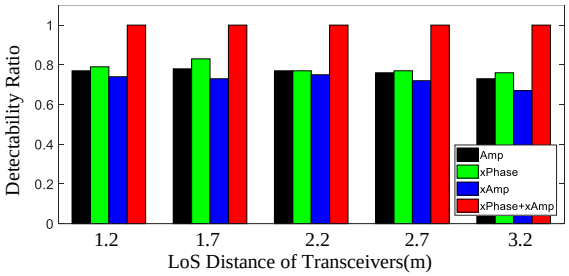


Fig. 14. The impact of LoS distance on the complementarity. The Amp, xPhase, xAmp are the amplitude of single antenna, the phase of CM, the amplitude of CM for short, respectively.

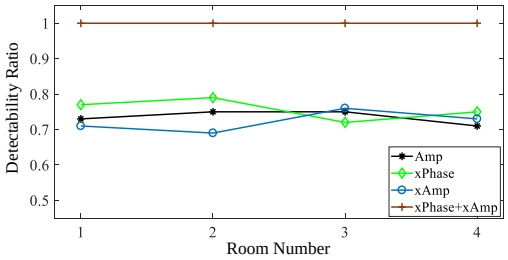


Fig. 15. The impact of environments on the complementarity in 4 rooms: 1) an empty hall room, 2) a living room, 3) a small bedroom, 4) a large bedroom.

from which we can effectively extract respiration rate in a certain setting when using amplitude (phase) with one sub-carrier, $N_{all}$ is the total number of collected CSI measurements in that setting. For each experimental setting, we present the detectability ratio of: 1) CSI amplitude of one antenna; 2) phase of CM; 3) amplitude of CM; 4) combined phase and amplitude of CM. Please note that 1) is the method taken from [33] which we include here as a comparison baseline.

*6.3.1 Impact of the LoS of the transceivers.* In this experiment, we choose a large bedroom to study the complementarity under various LoS distance of the transceivers. A subject is lying on the bed, and the transceivers are placed at two sides of the bed. The LoS distance of the transceivers increases gradually from 1.2 m to 3.2 m, and each time it increases by 0.5 m. Once the LoS is determined, we conduct a set of experiments in a similar way as did in Sec. 6.2. Please note that, in the scenario where a subject is lying, the antennas are set horizontally as in [33]. Thus we adjust the height of antennas gradually during the period in which the reflection path length changes two wavelengths. The case that a subject is near to or far from to the LoS are both taken into consideration as the same as the experiments in Sec. 4.4. In this scenario, the height of antennas is set to 1.08 m (1.91 m), corresponding to the near (far) case.

Fig. 14 presents the detectability ratio for respiration using phase (amplitude) under different LoS, namely 1.2 m, 1.7 m, 2.2 m, 2.7 m, and 3.2 m, respectively, when there is a single person lying on bed. Overall, we observe that, under different LoS, when only CSI amplitude of one antenna is used, about 76% of CSI measurements are detectable. That is to say, using amplitude of one antenna fails to extract respiration rate in 24% of CSI measurements. And the detectability ratio of phase/amplitude of CM is about 79% and 72%, respectively. Thus, when the phase and amplitude of CM is individually uesd for respiration sensing, blind spots still exist. We also find that, the detectability ratio of phase/amplitude differs in different LoS. However, if both phase and amplitude of CM are used, 100% of the CSI measurements are detectable. This suggests that, the complementarity of phase and amplitude of CM still holds under different LoS distance of the transceivers.

*6.3.2 Impact of the Environment.* In the experiment, we evaluate the complementarity in four different rooms: 1) an empty hall room, 2) a living room, 3) a small bedroom, 4) a large bedroom with the same experimental set-up (the LoS distance and the relative distance between subject and transceivers): In all four set-ups, the LoS of transceiver is fixed to 2 m, and the distance of subject to LoS is fixed to 1.5 m. As we did before, we move the antennas outward gradually until the reflected path length changes two wavelengths.

Fig. 15 presents the detectability ratio when using phase (amplitude) for the same set-up in four different rooms. We observe that, by exploiting both the phase and amplitude of CM, respiration rate can be extracted effectively for 100% of CSI measurements. However, blind spots exist if phase and amplitude is used individually.

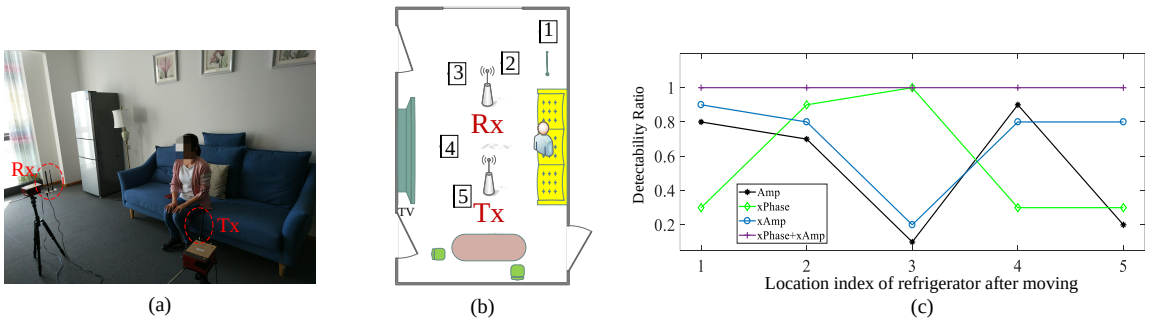


Fig. 16. The impact of environmental changes on the complementarity. (a) Experimental setting. (b) We change the environment by moving the refrigerator to 5 different positions. (c) Experimental result of the detectability ratio of the 5 environmental changes.

The experimental results suggest that, the complementarity of phase and amplitude of CM holds across different environments.

*6.3.3 Impact of Environmental Change.* In the last experiment, we study the impact of environmental changes on the complementarity property with commodity WiFi by moving static object in the environment. As shown in Fig. 16 (a), the experiment is conducted in a living room and a subject is sitting on a sofa. We fix the position of transceivers and move the refrigerator around to simulate the environmental changes. Since the refrigerator is made of metal, it is a perfect signal reflector and introduce a significant static component compared with other furnitures such as a sofa. We change the environment by moving the refrigerator to 5 different positions as shown in Fig. 16 (b). We collect 10 respiration CSI measurements at each refrigerator position, thus 50 CSI measurements are collected totally.

Fig. 16 (c) presents the detectability ratio for all 50 collected CSI measurements. We can see that, when phase and amplitude of CM are both used, we can extract respiration rate effectively for all the environmental changes. However, use amplitude or phase individually fail to ensure full respiration detection from all 50 CSI measurements. The results suggest that, using amplitude of a signal antenna for respiration sensing is subject to the environmental changes, while the complementarity of phase and amplitude of CM is resilient to environmental change.

The above experimental results show that, by exploiting the complementarity of phase and amplitude, full respiration detection is guaranteed under various LoS of transceivers in different environments and the complementarity property is resilient to environmental change. Thus, our approach outperforms the existing WiFi-based approaches using either amplitude of one antenna [22, 24, 33, 34] or phase difference between two RX antennas [36, 37], and it has great potential for real-world deployment.

## 7 LIMITATION AND DISCUSSION

In this section, we present and discuss several limitations in this work.

### 7.1 Multiple Subjects

Prior work extracts respiration rate from CSI amplitude for multiple subjects applying FFT or MUSIC methods [33, 36]. However, if a person is located in an amplitude-undetectable region, it may fail to detect respiration. This paper focuses on monitoring respiration for a single subject in a room. However, tracking respiration for multiple subjects can be made possible with a similar approach. Even for multiple subjects' situation, we know at least

one of amplitude and phase pairs contains their respiration rate information. The difficulty is to determine which pair contains the respiration rate we want. A potential solution could be, for example, to separate respiration information of two subjects, namely $A$ and $B$, we can arrange $A$ to an amplitude-undetectable area, and arrange $B$ to a phase-undetectable area. In this case, $B$'s respiration rate can be extracted from amplitude information, and $A$'s respiration rate can be extracted from phase information. Leveraging on the WiFi CSI phase and amplitude complementary nature, we can identify the two streams so as to determine different subjects. Anyway, monitoring respiration for multiple subjects reliably is challenging and hence we leave for our future work.

### 7.2 Respiration Sensing Range

The sensing range of a WiFi-based respiration system depends on many aspects, e.g., transmitting power, the automatic gain control of RF front, the gain of transmitter antenna and receiver antenna as well as the subject orientation. Under our current experiment settings, for a subject sitting on a chair facing the transceivers, while LoS is 1.2 m, the empirical sensing range beyond which full respiration detection is guaranteed with commodity WiFi is 1.7 m away from LoS. When LoS increases to 2 m, the sensing range is 2.4 m. The current sensing range is enough to cover a typical room if the subject faces the transceivers. However, with subject orientation changing, the sensing range may decrease dramatically, since the chest displacement during respiration is quite small in the mediolateral dimensions (around 1 mm). For example, while LoS is 1.2 m and the side of subject is facing the transceivers, the sensing range is about 0.8 m away from LoS. This sensing range limits the practical use of our system. To increase sensing range, we can deploy more WiFi devices so that the subject is facing at least one transceiver pair. We need quantitative study to achieve further sensing range which we leave for our future work.

### 7.3 Subject Posture and Activity

Our system requires a subject to keep still during respiration detection. While the subject is performing other activities such as drinking and walking, FullBreathe fails to detect respiration from WiFi signals since chest movement will be largely affected by significant body movement. The limitation is due to multi-path effects resulted from other body parts. Please note that, while chest movement due to respiration is periodical, the movement from other body parts is generally not periodical. Therefore, to some degree, we can alleviate the problem by identifying and discarding the CSI data when it is greatly affected by the movement of other body parts.

## 8 CONCLUSION

Contactless WiFi-based respiration monitoring systems are promising for daily home use. Existing work reveals that respiration sensing performance varies in different locations, and the detectable and undetectable areas are alternatively distributed according to the Fresnel zone model. In this paper, we address the blind spot problem in respiration detection, and discover that the CSI amplitude and phase information are complementary to each other for minute movement sensing such as respiration. Further, the complementarity is extended to commodity WiFi by using conjugate multiplication of the CSI between two receiver antennas. We then design and implement a real-time system for full respiration detection by compensating CSI amplitude with CSI phase with commodity WiFi. Our evaluation shows that our system FullBreathe ensures full respiration detection with consistent performance regardless of human location and environments, and it is resilient to environmental changes.

## ACKNOWLEDGMENTS

This research is supported by National Key Research and Development Plan under Grant No.2016YFB1001200, and Peking University Information Technology Institute (Tianjin Binhai).

## REFERENCES


[1] [n. d.]. WARP Project. ([n. d.]). http://warpproject.org

[2] Heba Abdelnasser, Khaled A Harras, and Moustafa Youssef. 2015. UbiBreathe: A ubiquitous non-invasive WiFi-based breathing estimator. In *Proceedings of the 16th ACM International Symposium on Mobile Ad Hoc Networking and Computing*. ACM, 277–286.

[3] Fadel Adib, Hongzi Mao, Zachary Kabelac, Dina Katabi, and Robert C Miller. 2015. Smart homes that monitor breathing and heart rate. In *Proceedings of the 33rd annual ACM conference on human factors in computing systems*. ACM, 837–846.

[4] Laura Anitori, Ardjan de Jong, and Frans Nennie. 2009. FMCW radar for life-sign detection. In *Radar Conference, 2009 IEEE*. IEEE, 1–6.

[5] Khadija Baba, Lahcen Bahi, and Latifa Ouadif. 2014. Enhancing geophysical signals through the use of Savitzky-Golay filtering method. *Geofísica internacional* 53, 4 (2014), 399–409.

[6] Marek Bartula, Timo Tigges, and Jens Muehlsteff. 2013. Camera-based system for contactless monitoring of respiration. In *Engineering in Medicine and Biology Society (EMBC), 2013 35th Annual International Conference of the IEEE*. IEEE, 2672–2675.

[7] David E Bloom, Elizabeth Cafiero, Eva Jané-Llopis, Shafika Abrahams-Gessel, Lakshmi Reddy Bloom, Sana Fathima, Andrea B Feigl, Tom Gaziano, Ali Hamandi, Mona Mowafi, et al. 2012. *The global economic burden of noncommunicable diseases*. Technical Report. Program on the Global Demography of Aging.

[8] Olga Boric-Lubecke, Geert Awater, and Victor M Lubecke. 2003. Wireless LAN PC card sensing of vital signs. In *Wireless Communication Technology, 2003. IEEE Topical Conference on*. IEEE, 206–207.

[9] Amy Diane Droitcour et al. 2006. *Non-contact measurement of heart and respiration rates with a single-chip microwave doppler radar*. Ph.D. Dissertation. Citeseer.

[10] Amy D Droitcour, Olga Boric-Lubecke, and Gregory TA Kovacs. 2009. Signal-to-noise ratio in Doppler radar system for heart and respiratory rate measurements. *IEEE transactions on microwave theory and techniques* 57, 10 (2009), 2498–2507.

[11] Amy D Droitcour, Olga Boric-Lubecke, Victor M Lubecke, Jenshan Lin, and Gregory TA Kovacs. 2004. Range correlation and I/Q performance benefits in single-chip silicon Doppler radars for noncontact cardiopulmonary monitoring. *IEEE Transactions on Microwave Theory and Techniques* 52, 3 (2004), 838–848.

[12] Hulya Gokalp and Malcolm Clarke. 2013. Monitoring activities of daily living of the elderly and the potential for its use in telecare and telehealth: a review. *TELEMEDICINE and e-HEALTH* 19, 12 (2013), 910–923.

[13] Igor Immoreev and Teh-Ho Tao. 2008. UWB radar for patient monitoring. *IEEE Aerospace and Electronic Systems Magazine* 23, 11 (2008), 11–18.

[14] Yakup Kilic, Henk Wymeersch, Arjan Meijerink, Mark J Bentum, and William G Scanlon. 2014. Device-free person detection and ranging in UWB networks. *IEEE journal of selected topics in signal processing* 8, 1 (2014), 43–54.

[15] Manikanta Kotaru, Kiran Joshi, Dinesh Bharadia, and Sachin Katti. 2015. Spotfi: Decimeter level localization using wifi. In *ACM SIGCOMM Computer Communication Review*, Vol. 45. ACM, 269–282.

[16] Antonio Lazaro, David Girbau, and Ramon Villarino. 2010. Analysis of vital signs monitoring using an IR-UWB radar. *Progress In Electromagnetics Research* 100 (2010), 265–284.

[17] Changzhi Li, Victor M Lubecke, Olga Boric-Lubecke, and Jenshan Lin. 2013. A review on recent advances in Doppler radar sensors for noncontact healthcare monitoring. *IEEE Transactions on microwave theory and techniques* 61, 5 (2013), 2046–2060.

[18] Changzhi Li, Yanming Xiao, and Jenshan Lin. 2007. Design guidelines for radio frequency non-contact vital sign detection. In *Engineering in Medicine and Biology Society, 2007. EMBS 2007. 29th Annual International Conference of the IEEE*. IEEE, 1651–1654.

[19] Xiang Li, Shengjie Li, Daqing Zhang, Jie Xiong, Yasha Wang, and Hong Mei. 2016. Dynamic-music: accurate device-free indoor localization. In *Proceedings of the 2016 ACM International Joint Conference on Pervasive and Ubiquitous Computing*. ACM, 196–207.

[20] Xiang Li, Daqing Zhang, Qin Lv, Jie Xiong, Shengjie Li, Yue Zhang, and Hong Mei. 2017. IndoTrack: Device-Free Indoor Human Tracking with Commodity Wi-Fi. *Proceedings of the ACM on Interactive, Mobile, Wearable and Ubiquitous Technologies* 1, 3 (2017), 72.

[21] James C Lin. 1975. Noninvasive microwave measurement of respiration. *Proc. IEEE* 63, 10 (1975), 1530–1530.

[22] Jian Liu, Yan Wang, Yingying Chen, Jie Yang, Xu Chen, and Jerry Cheng. 2015. Tracking vital signs during sleep leveraging off-the-shelf wifi. In *Proceedings of the 16th ACM International Symposium on Mobile Ad Hoc Networking and Computing*. ACM, 267–276.

[23] Xuefeng Liu, Jiannong Cao, Shaojie Tang, and Jiaqi Wen. 2014. Wi-Sleep: Contactless sleep monitoring via WiFi signals. In *Real-Time Systems Symposium (RTSS), 2014 IEEE*. IEEE, 346–355.

[24] Xuefeng Liu, Jiannong Cao, Shaojie Tang, Jiaqi Wen, and Peng Guo. 2016. Contactless respiration monitoring via off-the-shelf WiFi devices. *IEEE Transactions on Mobile Computing* 15, 10 (2016), 2466–2479.

[25] C Lowanichkiattikul, M Dhanachai, C Sitathanee, S Khachonkham, and P Khaothong. 2016. Impact of chest wall motion caused by respiration in adjuvant radiotherapy for postoperative breast cancer patients. *SpringerPlus* 5, 1 (2016), 144.

[26] O Boric Lubecke, P-W Ong, and VM Lubecke. 2002. 10 GHz Doppler radar sensing of respiration and heart movement. In *Bioengineering Conference, 2002. Proceedings of the IEEE 28th Annual Northeast*. IEEE, 55–56.

[27] L Robert Mogue and Boerje Rantala. 1988. Capnometers. *Journal of clinical monitoring* 4, 2 (1988), 115–121.

[28] Rita Paradiso. 2003. Wearable health care system for vital signs monitoring. In *Information Technology Applications in Biomedicine, 2003. 4th International IEEE EMBS Special Topic Conference on*. IEEE, 283–286.

[29] Yanzhi Ren, Chen Wang, Jie Yang, and Yingying Chen. 2015. Fine-grained sleep monitoring: Hearing your breathing with smartphones. In *Computer Communications (INFOCOM), 2015 IEEE Conference on*. IEEE, 1194–1202.

[30] Peter J Schreier and Louis L Scharf. 2010. *Statistical signal processing of complex-valued data: the theory of improper and noncircular signals*. Cambridge University Press.

[31] Nastaran Hesam Shariati and Edmond Zahedi. 2005. Comparison of selected parametric models for analysis of the photoplethysmographic signal. In *Computers, Communications, & Signal Processing with Special Track on Biomedical Engineering, 2005. CCSP 2005. 1st International Conference on*. IEEE, 169–172.

[32] Swaroop Venkatesh, Christopher R Anderson, Natalia V Rivera, and R Michael Buehrer. 2005. Implementation and analysis of respiration-rate estimation using impulse-based UWB. In *Military Communications Conference, 2005. MILCOM 2005. IEEE*. IEEE, 3314–3320.

[33] Hao Wang, Daqing Zhang, Junyi Ma, Yasha Wang, Yuxiang Wang, Dan Wu, Tao Gu, and Bing Xie. 2016. Human respiration detection with commodity wifi devices: do user location and body orientation matter?. In *Proceedings of the 2016 ACM International Joint Conference on Pervasive and Ubiquitous Computing*. ACM, 25–36.

[34] Pei Wang, Bin Guo, Tong Xin, Zhu Wang, and Zhiwen Yu. 2017. TinySense: Multi-user respiration detection using Wi-Fi CSI signals. In *e-Health Networking, Applications and Services (Healthcom), 2017 IEEE 19th International Conference on*. 1–6.

[35] Wei Wang, Alex X Liu, Muhammad Shahzad, Kang Ling, and Sanglu Lu. 2015. Understanding and modeling of wifi signal based human activity recognition. In *Proceedings of the 21st Annual International Conference on Mobile Computing and Networking*. ACM, 65–76.

[36] Xuyu Wang, Chao Yang, and Shiwen Mao. 2017. PhaseBeat: Exploiting CSI phase data for vital sign monitoring with commodity WiFi devices. In *Distributed Computing Systems (ICDCS), 2017 IEEE 37th International Conference on*. IEEE, 1230–1239.

[37] Xuyu Wang, Chao Yang, and Shiwen Mao. 2017. Tensorbeat: Tensor decomposition for monitoring multiperson breathing beats with commodity WiFi. *ACM Transactions on Intelligent Systems and Technology (TIST)* 9, 1 (2017), 8.

[38] Kajiro Watanabe, Takashi Watanabe, Harumi Watanabe, Hisanori Ando, Takayuki Ishikawa, and Keita Kobayashi. 2005. Noninvasive measurement of heartbeat, respiration, snoring and body movements of a subject in bed via a pneumatic method. *IEEE transactions on biomedical engineering* 52, 12 (2005), 2100–2107.

[39] Chenshu Wu, Zheng Yang, Zimu Zhou, Xuefeng Liu, Yunhao Liu, and Jiannong Cao. 2015. Non-invasive detection of moving and stationary human with wifi. *IEEE Journal on Selected Areas in Communications* 33, 11 (2015), 2329–2342.

[40] Dan Wu, Daqing Zhang, Chenren Xu, Hao Wang, and Xiang Li. 2017. Device-Free WiFi Human Sensing: From Pattern-Based to Model-Based Approaches. *IEEE Communications Magazine* 55, 10 (2017), 91–97.

[41] Dan Wu, Daqing Zhang, Chenren Xu, Yasha Wang, and Hao Wang. 2016. WiDir: walking direction estimation using wireless signals. In *Proceedings of the 2016 ACM International Joint Conference on Pervasive and Ubiquitous Computing*. ACM, 351–362.

[42] Yanming Xiao, Jenshan Lin, Olga Boric-Lubecke, and M Lubecke. 2006. Frequency-tuning technique for remote detection of heartbeat and respiration using low-power double-sideband transmission in the Ka-band. *IEEE Transactions on Microwave Theory and Techniques* 54, 5 (2006), 2023–2032.

[43] Nan Yu, Wei Wang, Alex X Liu, and Lingtao Kong. 2018. QGesture: Quantifying Gesture Distance and Direction with WiFi Signals. In *Proceedings of the ACM on Interactive, Mobile, Wearable and Ubiquitous Technologies*. ACM.

[44] Daqing Zhang, Hao Wang, and Dan Wu. 2017. Toward centimeter-scale human activity sensing with Wi-Fi signals. *Computer* 50, 1 (2017), 48–57.

[45] Jincao Zhu, Youngbin Im, Shivakant Mishra, and Sangtae Ha. 2017. Calibrating Time-variant, Device-specific Phase Noise for COTS WiFi Devices. In *Proceedings of the 15th ACM Conference on Embedded Network Sensor Systems*. ACM, 15.

[46] Yiwei Zhuo, Hongzi Zhu, Hua Xue, and Shan Chang. 2017. Perceiving accurate CSI phases with commodity WiFi devices. In *INFOCOM 2017-IEEE Conference on Computer Communications, IEEE*. IEEE, 1–9.